SAR Simulation report for Simultaneous SAR Calculation

Table of Contents

1 Introduction

In addition to being able to be charged by a desktop WPT charger (puck), 2020 iPhone models (FCC IDs BCG-E3542A, BCG-E3543A,BCG-E3544A, BCG-E3545A,BCG-E3546A,BCG-E3547A, BCG-E3539A, BCG-E3540A, BCG-E3541A, BCG-E3548A, BCG-E3549A, BCG-E3550A), also support WPT charging function at 360 kHz to charge accessories. Currently the only accessory that can be charged by iPhones is an external potential apple accessory in future.

Per §1.1310, iPhone WPT operating at 360 kHz demonstrates RF exposure compliance through field strength measurement. However, for simultaneous transmission analysis, a more accurate estimated SAR value for the WPT transmitter is needed. This report uses computational modeling to arrive at an estimate of the maximum SAR value for the 2020 series of iPhones described in the paragraph above and as approved via KDB inquiry with FCC.

The charging session only occurs when the phone is connected to an AC power outlet. However, due to the potential apple accessory in future and the phone being held in place by magnets, it is envisioned that customers may use the charging function in a portable use condition, for example, charging the battery while making a call or texting. Therefore, to be conservative we evaluate iPhone WPT transmitter as a mixed mobile/portable device. Future designs and accessories may support true portable use condition, with the host-client pair able to be placed in a pocket or backpack. In those cases, a body-worn exposure assessment would be conducted.

At 360 kHz operating frequency, we have found that the near-field H field strength could be high, taking up most RF exposure budget when doing simultaneous transmission analysis. Therefore, since SAR is applicable for portable devices operating 100 kHz – 6 GHz, we use SAR numerical modeling to arrive at an estimated SAR value, due to the unavailability of SAR measurement tools.

The following sections describe the modeling, measured H-field, simulated H-field, and simulated SAR.

2 Wireless Power Transfer System

The wireless power transmission system consists of a transmitting coil with 13 turns and measures 9.06 uH nominally in free air. The receiver coil consists of 11 turns and measures 7.5 uH nominally in free air. Both coils are wound spirally. Below are the details of the Tx Coil, which is used in all of the iPhone models described in section 1 of this report.

Tx Winding Type	Spiral, 1 Layer, Stranded Wire
Turns	13
Inner Radius	10.06 mm
Outer Radius	21.35 mm
Cross section	Rectangular
Thickness	0.13 mm
Width	0.62 mm

Rx Winding Type	Spiral, 1 Layer, Stranded Wire
Turns	11
Inner Radius	10.9 mm
Outer Radius	18.9 mm
Cross section	Rectangular
Thickness	0.32 mm
Width	0.49 mm

Below are some key initial parameters used in the design that will be helpful in determining worst-case use for exposure. These are common to all of the iPhone models described in section 1 of this report.

Item	**Description**
Max Power Delivered	5 Watt
Functional On-body max offset	Refer to graph below
Operating Frequency	f_0 = 360 kHz
Communication Method	ASK -> Phone to Charger FSK -> Charger to Phone
Object Detection Mode	Magnetic + NFC

Refer to antenna location file for of all antennas in the phone, and how the WPT coil is separated from other antennas.

3 SAR Simulations Methodology

The following steps are taken to show the validity of the model used for SAR Simulations:

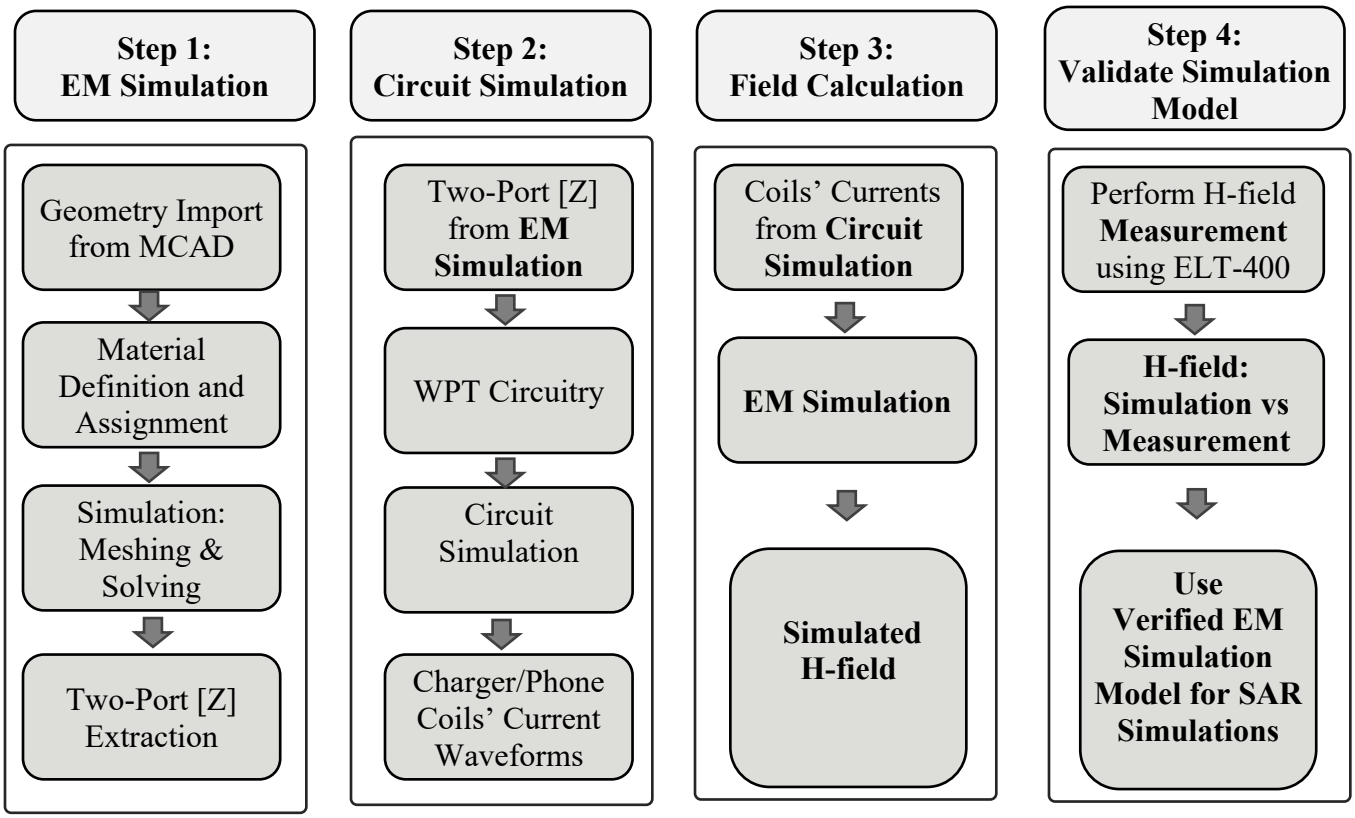

1) EM Simulation:
    a. Import a CAD model that represents the actual product in the simulation tool.
    b. Define material properties inside the product based on vendor's inputs.
    c. Extract two-port network impedance matrix ([Z]) from the simulation.
2) Circuit Simulation:
    a. Include the impedance matrix in the wireless power transfer (WPT) circuit model
    b. Run circuit simulation and extract coils' current waveforms
3) Field Calculations:
    a. Use the current waveforms to drive the EM simulation model.
    b. Calculate H-field from the simulation.
4) Validate Simulation Model:
    a. Measure H-field, and compare with simulation result
    b. Once a correlation is established, and model's accuracy is verified, this model will be used for computational exposure assessments (e.g., SAR simulations).

4 H-field Measurements

Narda EHP-200AC probe is used to measure the H-field above the EUT. This is an isotropic probe designed for accurate measurements of both electric and magnetic fields. The field sensors and the electric measuring circuitry are contained in a rugged housing. Separate 3-axis and total values are measured and displayed in real time by a PC through the optical fiber link with the measurement probe. Since the measurement probe provides a flat frequency response throughout the frequency range of 3 kHz to 10 MHz, no frequency- dependent amplitude weighting factors are applied to the measurement results.

Probe Specifications:

Model	EHP-200AC
Frequency	3 kHz – 30 MHz
Linearity	± 0.5 dB @ 1 MHz to full scale
Frequency Response	± 0.5 dB for Electric field ± 0.8 dB for Magnetic field
Dynamic Range	0.1 to 1000 V/m for Electric field 0.03 to 300 A/m for Magnetic field
Maximum frequency span	6 kHz to 30 MHz
Resolution Bandwidth (RBW) available	1 kHz, 3 kHz, 10 kHz, 30 kHz, 100 kHz, 300 kHz
Anisotropy	± 0.8 dB at 1 MHz
Dimensions	92 x 92 x 109 mm
Application	Electric and Magnetic field measurement

5 H-field Simulations

The Electromagnetics simulations are conducted using commercially available software ANSYS HFSS. In order to validate the simulation model, H-field measurements are made on the EUT (as explained above) and compared to the simulated model results. The validated model is then used for SAR simulations.

For the simulations, following Step 1, which is described above, the CAD file that represents the EUT is first imported. Then the proper material properties are assigned at the operating frequency (360 kHz). After the simulation is completed, the two-port network [Z] was extracted and used with the WPT circuit model. This WPT model includes the Phone (charger) as well as the accessory (potential apple accessory in future) rectifier circuit. Solving the circuit using ANSYS Circuit tool, the proper excitation per transmitter (charger) and receiver (potential apple accessory in future) coils are calculated. Later, these current waveforms are fed into the ANSYS HFSS to excite the coils and create H-field.
As shown below, the phone and accessory can be unintentionally forced by user to be laterally misaligned or vertically separated.

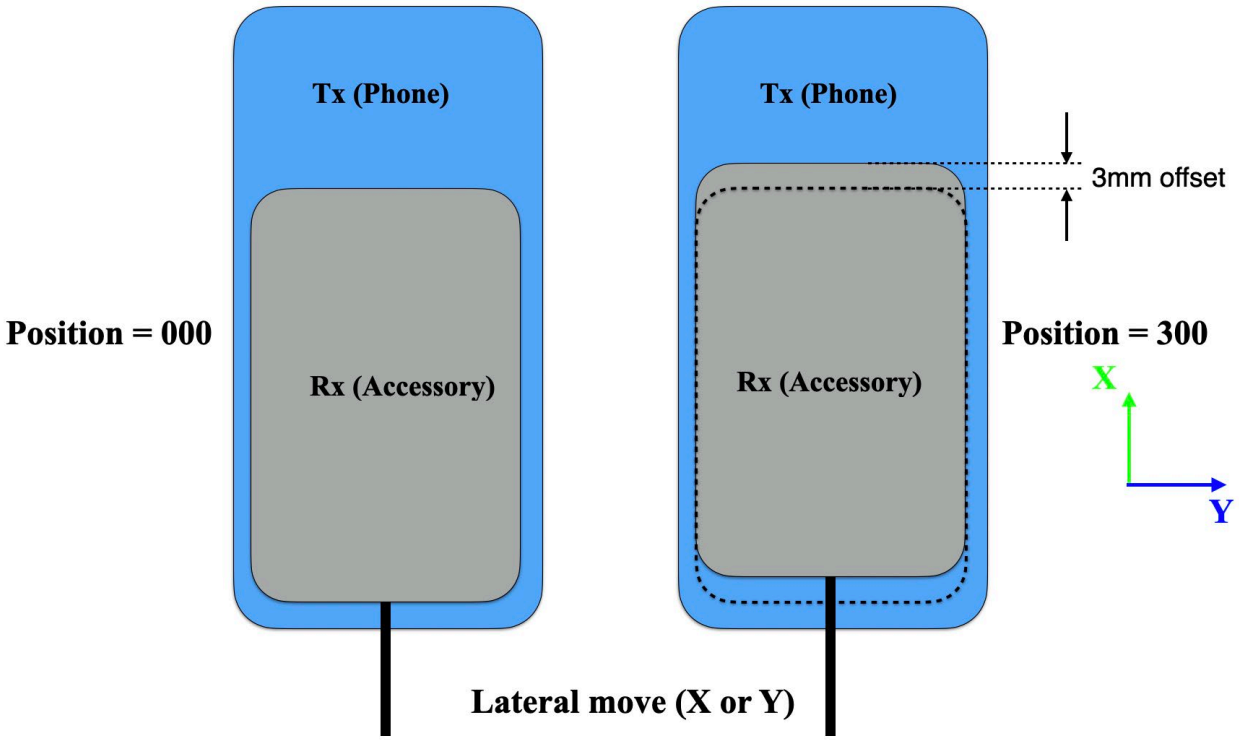

(a) Best Alignment (b) Misalignment alignment of 3mm

Vertical (z) move

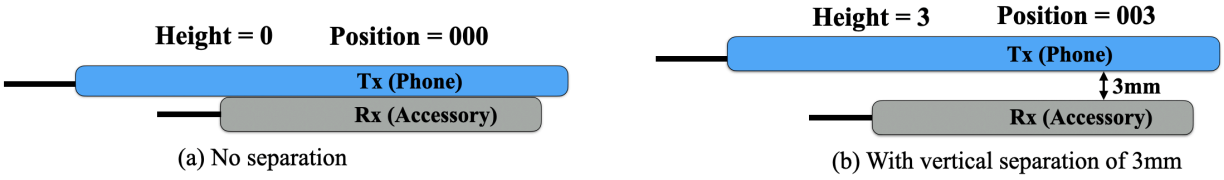

(a) No separation

(b) With vertical separation of 3mm

The misalignment and/or separation can change H-field's intensity and spatial distribution. Hence, several different misalignment and separation cases were selected and investigated to determine the worst-case scenario (i.e., highest H-field).
After simulating these cases, some will be selected and measured and used to benchmark the accuracy of the simulation model. Finally, a few cases will be selected for SAR simulation.

To this end, the simulation results are compared for the phone and battery side, below. The target power shows the maximum deliverable power per each case. For example, to be able to deliver a maximum power of 5 W to the accessory, the maximum offset is found to be either 2 mm radially on z = 2 mm plane. For each side, the H-field probe is in contact with the EUT, scanning an area of 100 by 200 mm^2 with step size of 5 mm. The maximum RMS H-field is reported in the tables (unit: A/m).
There is a good agreement between the simulation and measurement results. Also, as tables show, for aligned cases (i.e., zero lateral move), the phone side relatively shows more radiation. This is mainly because the metallic housing of the battery preforms as a good shield. While when there is a lateral misalignment, fields can leak from the sides and the H-field on the battery side becomes more.

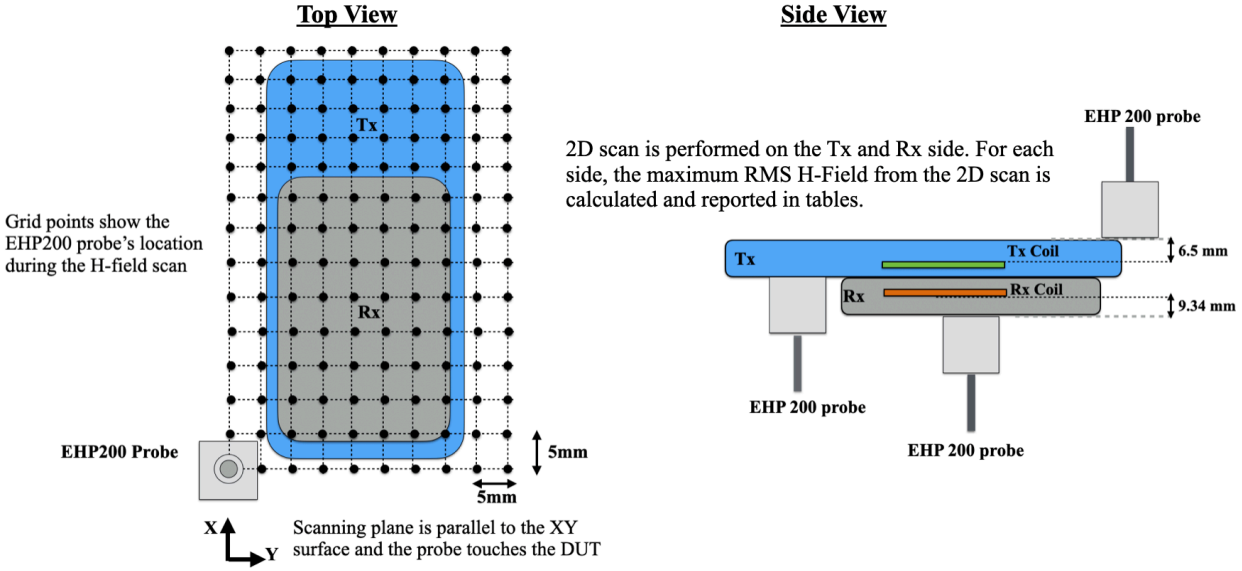

Phone side RMS H-field (A/m)

Phone's relative move (X,Y,Z) from Alignment (mm)	Target Power (W)	Simulated RMS H-field (A/m)	Measured H-field (A/m)
(0,0,0)	5	0.31	0.27
(2,0,2)	5	0.73	0.41
(3,0,3)	3	0.9	0.34

Puck side RMS H-field (A/m)

Phone's relative move (X,Y,Z) from Alignment (mm)	Target Power (W)	Simulated RMS H-field (A/m)	Measured H-field (A/m)
(0,0,0)	5	0.23	0.21
(2,0,2)	5	1.15	1.23
(3,0,3)	3	1.53	0.88

H-field measurements on all of the models described in section 1 of this report across various charging scenarios showed a variance in the maximum measured H-field of 0.75 A/m to 1.23 A/m, correlating very closely to the worst case values obtained through simulation and to the values in the tables above used to validate the simulation model.

6 SAR Simulations

The same model is then used for SAR calculations with a phantom added in contact with the EUT. The simulations are computed on a 96 core CPU server with an available RAM of 4 Terabytes. For this simulation, the model run takes approximately 8 hours to complete.

The following steps are used for accurate SAR calculations:

1) Elliptical phantom used in body exposure measurements is commercially available from SPEAG: Outer Dimensions of 600mm x 400mm x 150mm.
2) Homogeneous tissue material is used as liquid for desired frequency.
3) Power loss in phantom is calculated.
4) Divide power loss by mass density to calculate SAR.

$$SAR = \frac{P_l}{\rho}$$

$$P_l = \text{Power loss density}$$

$$\rho = \text{Mass density}$$

5) Point SAR is averaged over 1g or 10g tissue.

Human Tissue Material Properties at 360 kHz:
The worst-case scenario has been identified to be when a user is holding the device in hand and taking a call or holding the phone on their body while charging. The electrical properties for body and hand layers are shown below. Since the SAR phantom is homogenous, using the layers' properties, the worst-case scenario is selected and applied for the phantom properties. Therefore, for the SAR simulations, the phantom that has conductivity of 0.5 and permittivity of 5016 at the 360 kHz operating frequency is used.

Electrical Properties:
Based on our research this is what we recommend for er and sigma values for body layers

Tissue	Thickness **(mm)**	Permittivity	Conductivity **(S/m)**
Skin	3	5016	0.16
Muscle	9	4666	0.5
Bone	20	1414	0.165
Worst case	100	5016	0.5

Based on our research this is what we recommend for er and sigma values for hand layers

Tissue	Thickness **(mm)**	Permittivity	Conductivity **(S/m)**
Skin	2	5016	0.16
Muscle	2	4666	0.5
Bone	15	1414	0.165
Worst case	100	5016	0.5

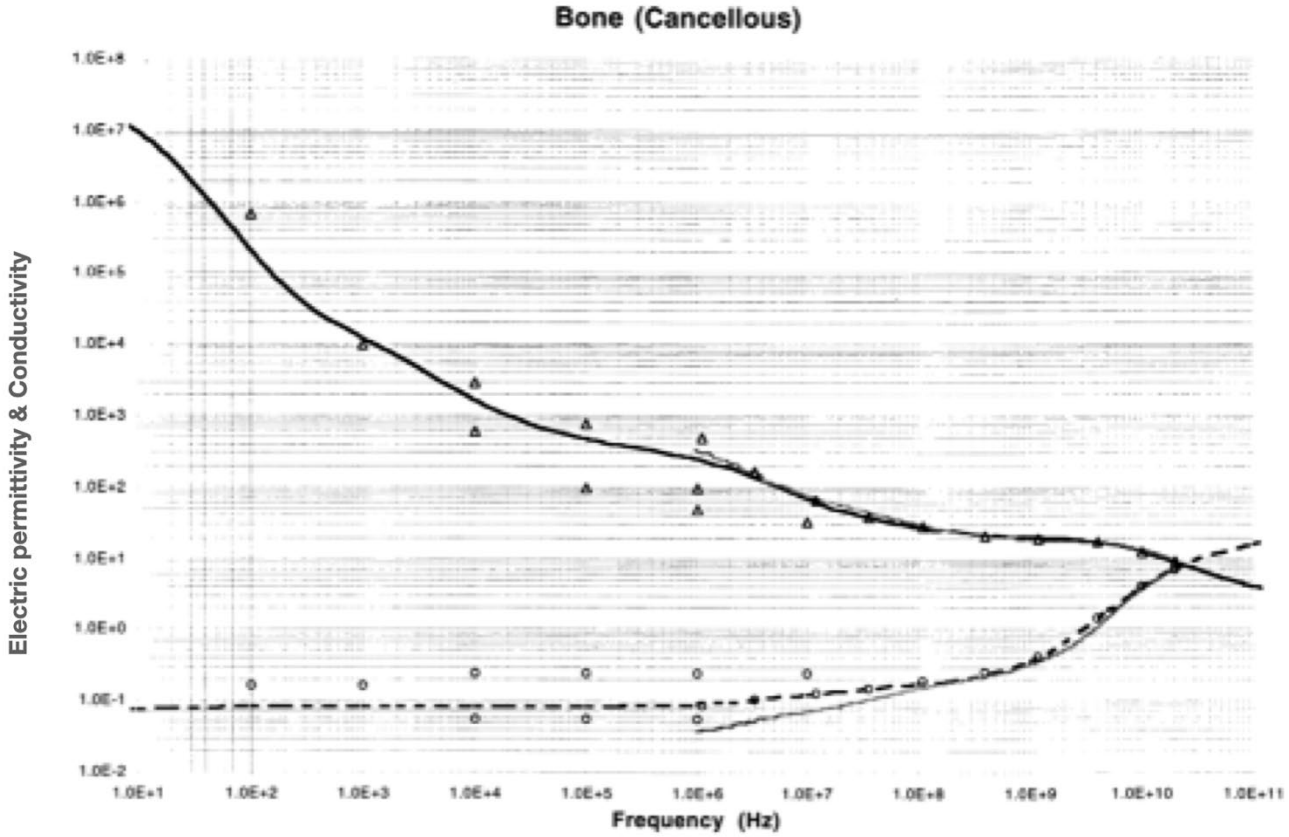
Bone (Cancellous)
Electric permittivity & Conductivity
1.0E+8
1.0E+7
1.0E+6
1.0E+5
1.0E+4
1.0E+3
1.0E+2
1.0E+1
1.0E+0
1.0E-1
1.0E-2
1.0E+1
1.0E+2
1.0E+3
1.0E+4
1.0E+5
1.0E+6
1.0E+7
1.0E+8
1.0E+9
1.0E+10
1.0E+11
Frequency (Hz)

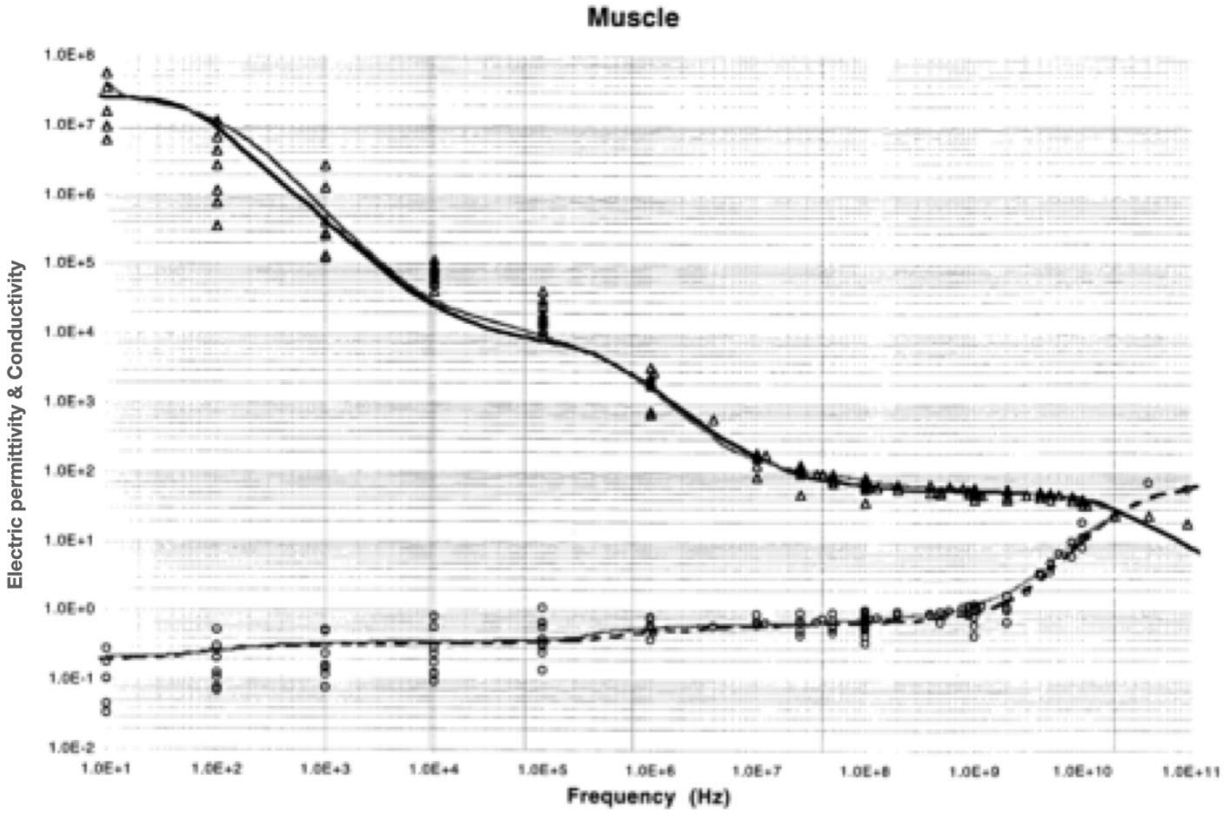
Muscle
Electric permittivity & Conductivity
1.0E+8
1.0E+7
1.0E+6
1.0E+5
1.0E+4
1.0E+3
1.0E+2
1.0E+1
1.0E+0
1.0E-1
1.0E-2
1.0E+1
1.0E+2
1.0E+3
1.0E+4
1.0E+5
1.0E+6
1.0E+7
1.0E+8
1.0E+9
1.0E+10
1.0E+11
Frequency (Hz)

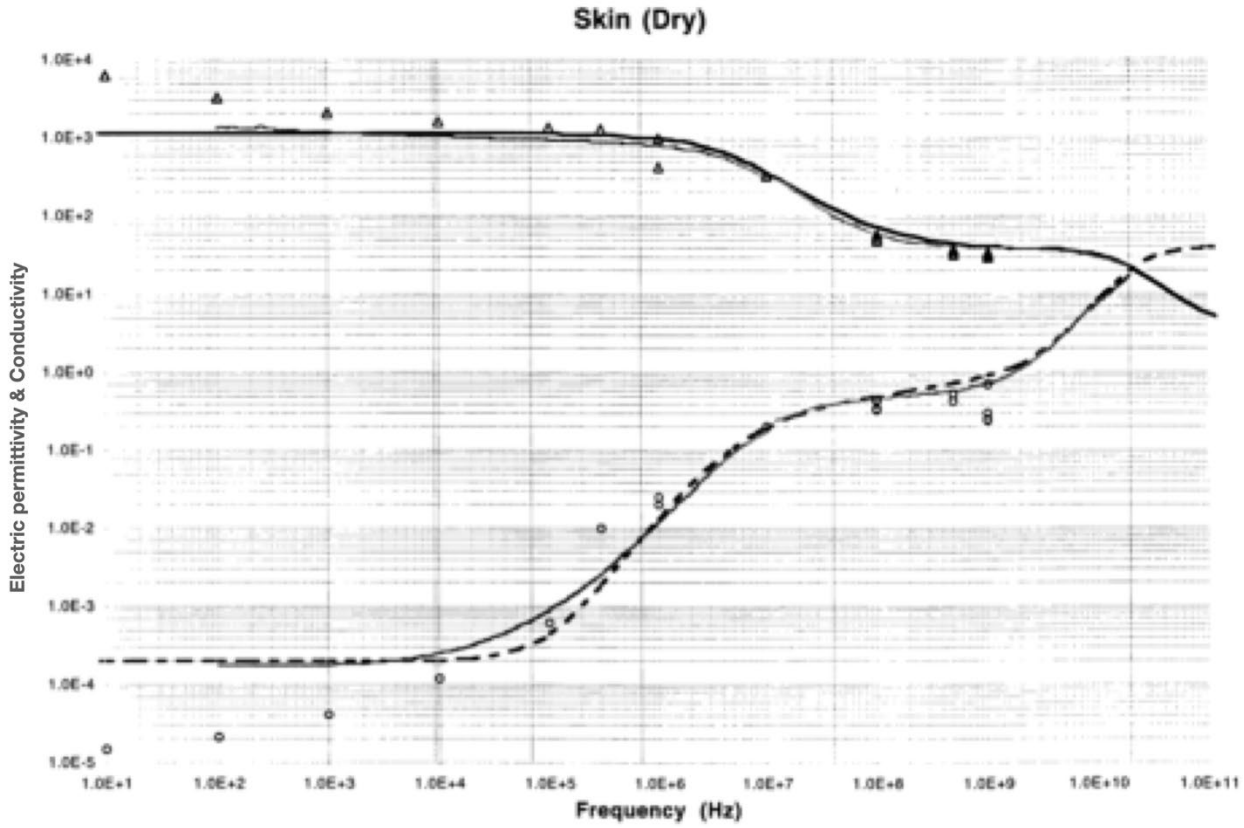

Mesh Adaptation:
HFSS adapts the mesh based on field strength. It is important to ensure the mesh is refined to capture SAR accurately. This can be done by using adaptive meshing available in HFSS.

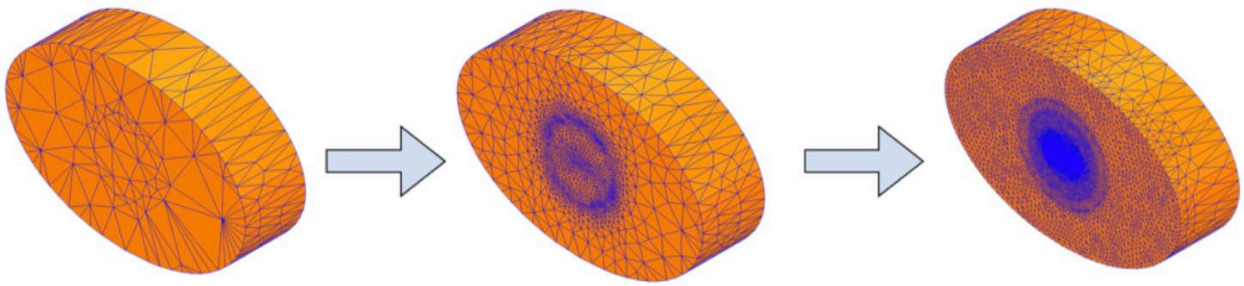

SAR Results:

Using the H-field simulation and measurement tables, two exposure cases were selected for SAR investigation. Considering that the phantom can be in contact with the phone or battery, there is a total of four scenarios.

> **Exposure Case 000 (a):** Nominal configuration with perfect alignment and phantom placed above the receiving unit
> **Exposure Case 000(b):** Nominal configuration with perfect alignment and phantom placed below the transmitting unit
> **Exposure Case 303 (a):** Misaligned configuration with the worst-case alignment and phantom placed above the receiving unit
> **Exposure Case 303 (b):** Misaligned configuration with the worst-case alignment and phantom placed below the transmitting unit

For all the exposure cases, dielectric properties (conductivity and permittivity) used for the phantoms are fixed as (permittivity: 5016, conductivity: 0.5).
The coil properties are also fixed, transmitting coil with 13 turns and measures 9.06 uH nominally in free air. The receiver coil consists of 11 turns and measures 7.5 uH nominally in free air. Both coils are wound spirally.
The following outputs are calculated and reported in the Table:

a. Peak spatial 1-gram average SAR in tissue.
b. Peak spatially averaged electric field in tissue. Electric field is spatially averaged in a contiguous tissue volume of 2 mm by 2 mm by 2 mm.

The simulation results for the four exposure cases are listed in the table, below.

Exposure Case	Description	Peak Spatial Average SAR (W/kg) Averaged over 1 gram	Peak Spatial Avg E (V/m) Averaged over 2x2x2 mm^3
Case 000 (a)	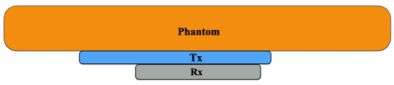	0.000001	0.14
Case 000 (b)	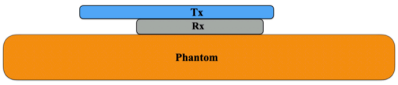	0.000000068	0.02
Case 303 (a)	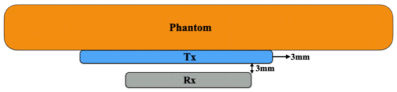	0.0000035	0.23
Case 303 (b)	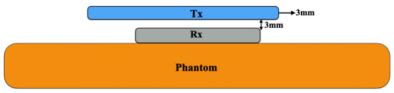	0.0000028	0.13

SAR plot (Bottom view) is shown below for Case303(a). The peak spatial 1-g average SAR is 0.0000035 W/kg.

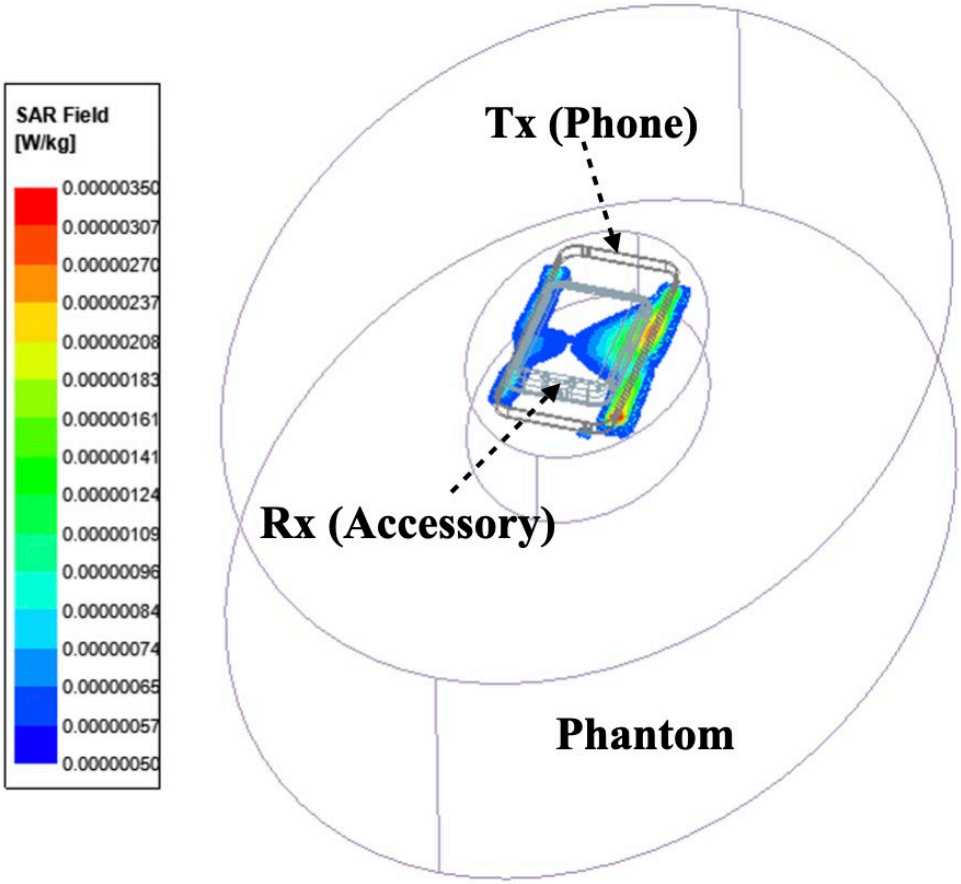

The side view is also presented, below.

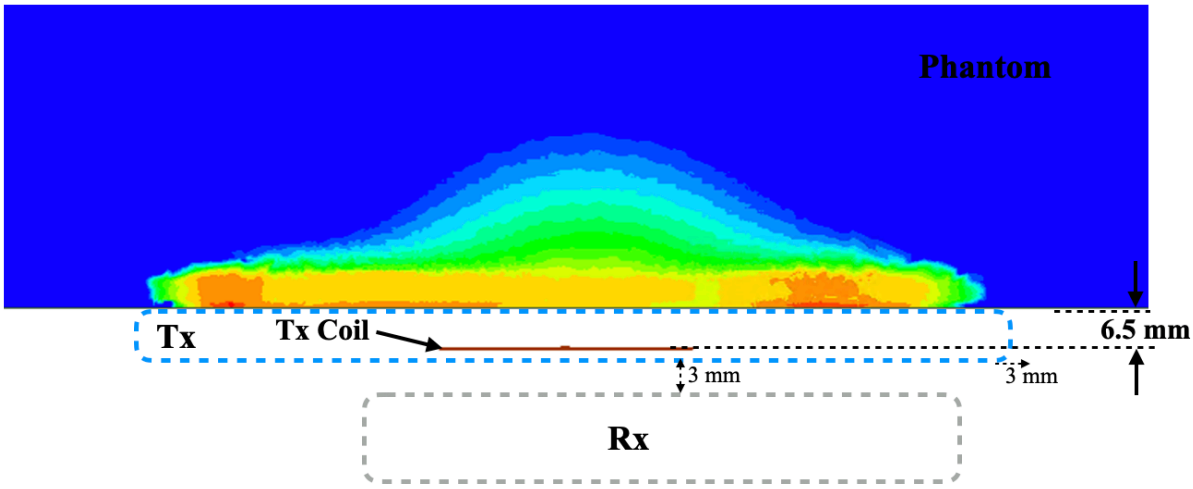

7 Impact of Housing Material and Size

The phones all share a common material for the back of the phone and while the edge material may be different (stainless steel versus aluminum) the separation distance of at least 1cm between the coil and the sides of the phones will not significantly impact the RF exposure values. This has been verified through H-field measurements as detailed in section 5.
In this section we studied the worst case orientation (303-a) for SAR simulations to see the impact of housing materials and housing size.

Housing Material:
The housing material on the edges were simulated twice, once as steel, the other as Aluminum. The Table below summarize the difference.

Model number	Housing Material	Peak Spatial Average SAR (W/kg) averaged over 1gm	Peak Spatial Average E (V/m) averaged over 2x2x2mm^3
A2172, BCG-E3542A A2402, BCG-E3543A A2403 / A2404 / A2405, BCG-E3544A	Aluminium	0.0000035	0.23
A2341, BCG-E3545A A2406, BCG-E3546A A2407 / A2408 / A2409: BCG-E3547A	Steel	0.0000046	0.24

The SAR plots comparison between Steel and Aluminum is shown below.

Model number	Housing Material	Peak Spatial Average SAR (W/kg) averaged over 1gm
A2172, A2402, A2403, A2404, A2405	Aluminum	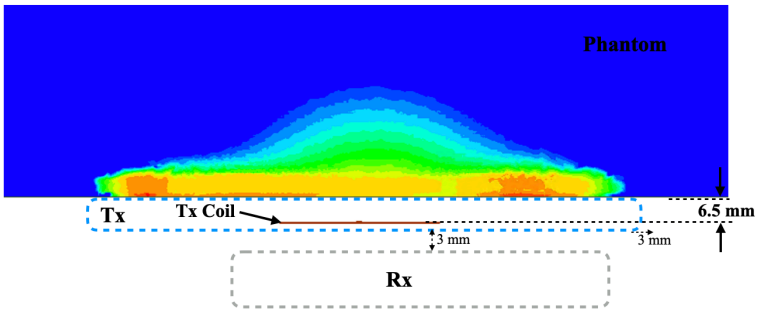
A2341, A2406, A2407, A2408, A2409	Steel	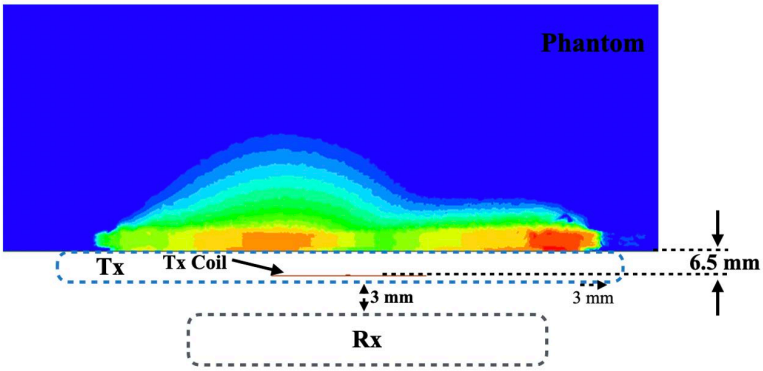

The SAR values produced from both housing is still very small (below 0.001% of the actual SAR limit), and that can be used to demonstrate there is no need to study different housing materials in details.

Housing size:

The phones for 2020 will have three different sizes as summarized in the sketched outlines below. FCC IDs BCG-E3542A, BCG-E3543A, BCG-E3544A, BCG-E3545A, BCG-E3546A, and BCG-E3547A on which the initial analysis was based have the mid-size dimensions. The largest form factor is for FCC IDs BCG-E3548A, BCG-E3549A, and BCG-E3550A and the smaller form factor is FCC IDs BCG-E3539A, BCG-E3540A, and BCG-E3541A.

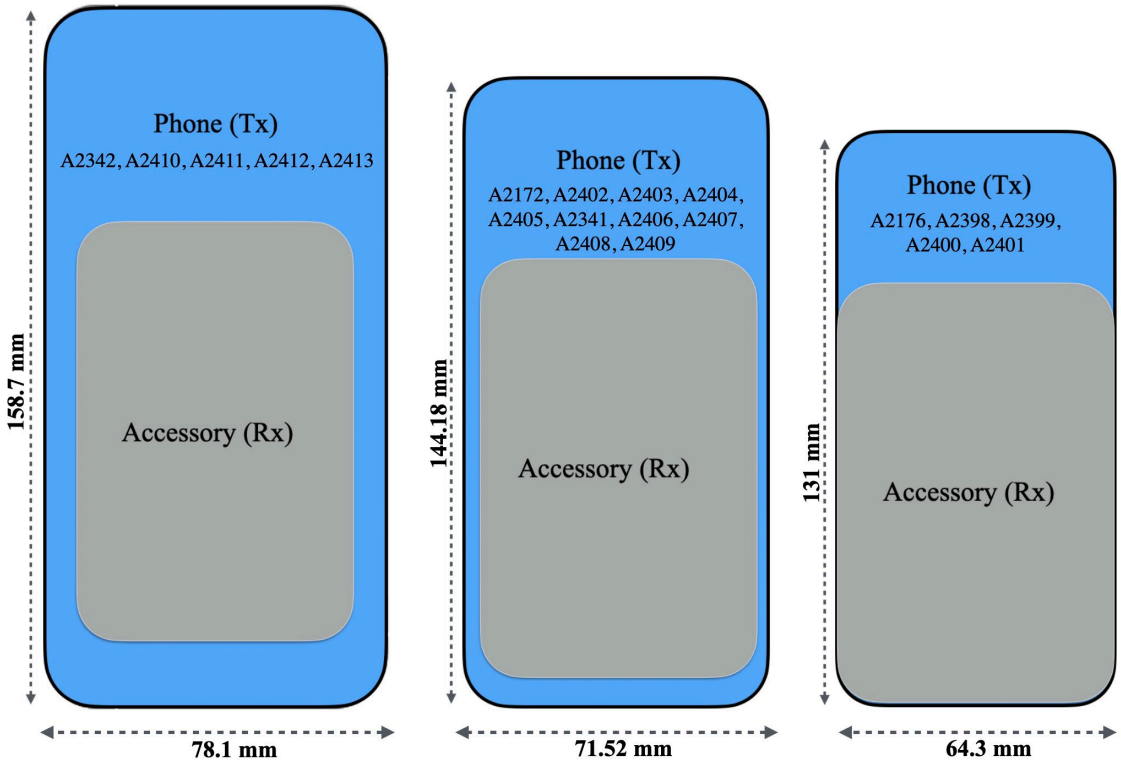

In this study we used the worst case orientation (303-a) form the initial analysis to study how SAR and E-field changes with different housing sizes.

The table below summarizes the results, and the SAR plots are shown for each size afterward

Model number	Housing Size (mm)	Peak Spatial Average SAR (W/kg) averaged over 1gm	Peak Spatial Average E (V/m) averaged over 2x2x2mm^3
A2172, A2402, A2403, A2404, A2405, A2341, A2406, A2407, A2408, A2409	71.52 x 144.18	0.0000046	0.24
A2342, A2410, A2411, A2412, A2413	78.1 x 158.7	0.0000024	0.23
A2176, A2398, A2399, A2400, A2401	64.3 x 131	0.0000100	0.32

The SAR plots comparison for the different form factors are shown below.

Model number	Housing Size (mm)	Peak Spatial Average SAR (W/kg) averaged over 1gm
A2172, A2402, A2403, A2404, A2405, A2341, A2406, A2407, A2408, A2409	71.52 x 144.18	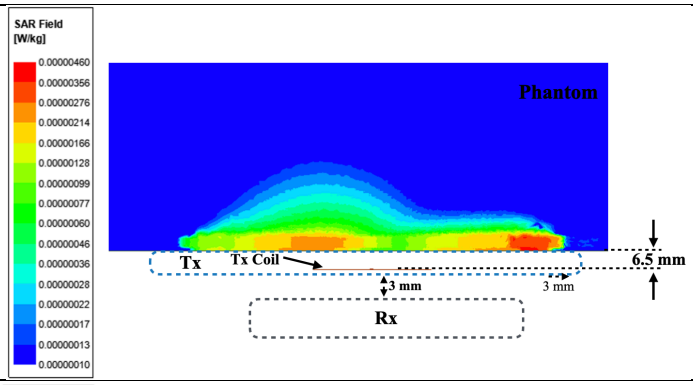
A2342, A2410, A2411, A2412, A2413	78.1 x 158.7	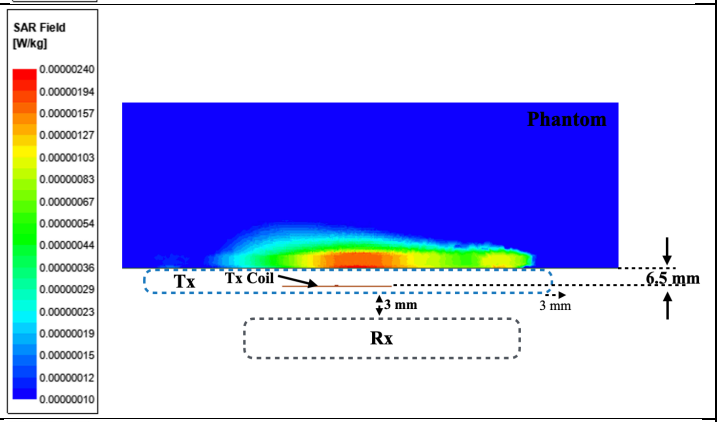
A2176, A2398, A2399, A2400, A2401	64.3 x 131	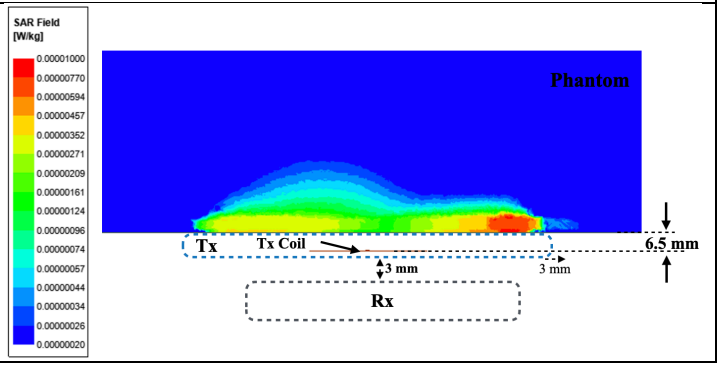

The Housing size is shown to have small impact on the SAR and E-field values. It can be observed that the computed SAR increases as housing size decreases, but the SAR numbers are still less than 0.001% of SAR limit of 1.6 W/Kg.

8 Summary

Based upon the above results, the accuracy of the SAR simulations is demonstrated by correlating H-field measurements to simulations. The validity of using this modeling and SAR computational method hence is established for iPhone models FCC IDs BCG-E3542A, BCG-E3543A, BCG-E3544A, BCG-E3545A, BCG-E3546A, BCG-E3547A, BCG-E3539A, BCG-E3540A, BCG-E3541A, BCG-E3548A, BCG-E3549A, BCG-E3550A. For the nominal case where the battery and the phone are aligned without any vertical separation, the highest peak spatial 1-gram average SAR is 0.0000100 W/Kg and the highest peak spatial average E field (i.e., averaged over a cube of 2 mm x 2 mm x 2 mm) is 0.32 V/m.

The low level of SAR (below 0.001% of the actual SAR limit) indicates that any contribution of the WPT operation to the overall RF exposure budget for the 2020 series of iPhones when operating close to the body is negligible and does not need to be considered in the SAR / Power Density calculations for assessing simultaneous transmissions.

9 Annex A: specific information for SAR computational modelling

1) Computation Resources

The models were simulated on a 96 core CPU server with an available RAM of 4 Terabytes. Each model variation took around 12 hours to complete. Based on the simulation profile, the minimum resources needed to finish these simulations will be approximately 8 core CPU with 512 GB of RAM. Using the minimum requirements simulation will likely take more time than 12 hours.

2) Algorithm implementing and validation

This section is divided into two parts. The code performance validation provides methods to determine that the finite-element algorithm in HFSS has been implemented correctly and works accurately within the constraints due to the finite numerical accuracy. It further determines the quality of absorbing boundary conditions and certain parts of the post processing algorithms that are part of HFSS. The second part has few canonical benchmarks. All benchmarks can be compared to analytical solutions of the physical problem or its numerical representation. The methods characterize the implementation of the finite-element algorithm used by HFSS in a very general way. They are defined such that it is not possible to tune the implementation for a particular benchmark or application without improving the overall quality of the code.

2.1) Code performance validation

2.1.1) Propagation homogeneous medium

A straight rectangular waveguide with ports on both ends is well suited as a first test of an implementation of the Finite-Element Method used by HFSS. The waveguide has a width of 20 mm, a height of 10 mm and a length of 300 mm. The waveguide is filled homogeneously with a material which, in three separate simulations, shall assume the following properties:

i. $\varepsilon r = 1$, $\sigma = 0$ S/m;
ii. $\varepsilon r = 2$, $\sigma = 0$ S/m;
iii. $Re(\varepsilon r) = 2$, $\sigma = 0.2$ S/m.

To verify that the mesh used by HFSS is independent of orientation, the waveguide has been rotated so that it is not parallel with any principal coordinate plane (XY, XZ, YZ). The waveguide is driven in the TE10 mode at 10 GHz. Reported are the magnitudes of S21 and S11, as well as the values of the real and imaginary parts of the propagation constant γ. The table 1, below provides the reference values [B1], acceptable result criteria, as well as the simulated results.

Table 1: Criteria for the waveguide evaluation

Re(ε_r)	1	2	2
σ	0	0	0.2
|S21| reference value	1	1	8.7 × 10-5
Criterion for |S21|	≥ 0.9999	≥ 0.9999	± 5 × 10-6
|S21| simulated results	1	1	8.7 × 10-5
|S11| reference value	0	0	0
Criterion for |S11|	≤ 0.003	≤ 0.003	≤ 0.003
|S11| simulated results	0	0	0
Re(γ) reference value	0	0	31.17 m-1
Criterion for Re(γ)	± 0.1 m-1	± 0.1 m-1	± 2%
Re(γ) simulated results	0	0	31.17
Im(γ) reference value	138.75 m-1	251.35 m-1	253.28 m-1
Criterion for Im(γ)	± 2%	± 2%	± 2%
Im(γ) simulated results	138.75	251.35	253.28

As is seen in the above table, HFSS easily meets the criteria for properly and accurately calculating the waveguide problem.

2.2.2) Planar dielectric boundary

In order to test the reflection of a plane wave by a dielectric boundary, a rectangular waveguide can again be used. It is well known that the TE10 mode can be thought of as a superposition of two plane waves [1]. Each wave's direction of propagation makes an angle θ with the axis of the wave guide, given by

$$\cos^2\theta = 1 - (c/2af)^2 \quad (1)$$

where c is the speed of light, a is the width of the wave guide and f is the frequency. Assuming the axis of the waveguide is the Z axis and assuming the waveguide is filled with vacuum for Z>0 and filled with dielectric 1 with complex relative permittivity εr for Z<0, Fresnel reflection coefficients for the TE and the TM cases, defined as ratios of electric field strengths, are given by [2]

$$R^{TE} = (k_{0,z} - k_{1,z}) / (k_{0,z} + k_{1,z}) \quad (2)$$

$$R^{TM} = (\varepsilon_r k_{0,z} - k_{1,z}) / (\varepsilon_r k_{0,z} + k_{1,z}) \quad (3)$$

where $k_{0,z}$ and $k_{1,z}$ denote the z component of the propagation vector of the plane wave in vacuum and in the dielectric, respectively. They can be evaluated through

$$k_{0,z} = k_0 \cos\theta \quad (4)$$
$$k_{1,z} = k_0 \sqrt{(\varepsilon_r - \sin^2\theta)} \quad (5)$$

Finally, ε_r is complex and is given by

$$\varepsilon_r = \mathrm{Re}(\varepsilon_r) - j\sigma/(2\pi f \varepsilon_0) \quad (6)$$

where $\mathrm{Re}(\varepsilon_r)$ denotes the real part of the relative permittivity and σ is the conductivity of the medium.
For this test, a 20 mm × 10 mm waveguide with a length of 60 mm, as shown in Figure 1, was created. The top half was filled with vacuum and the bottom half with dielectric.

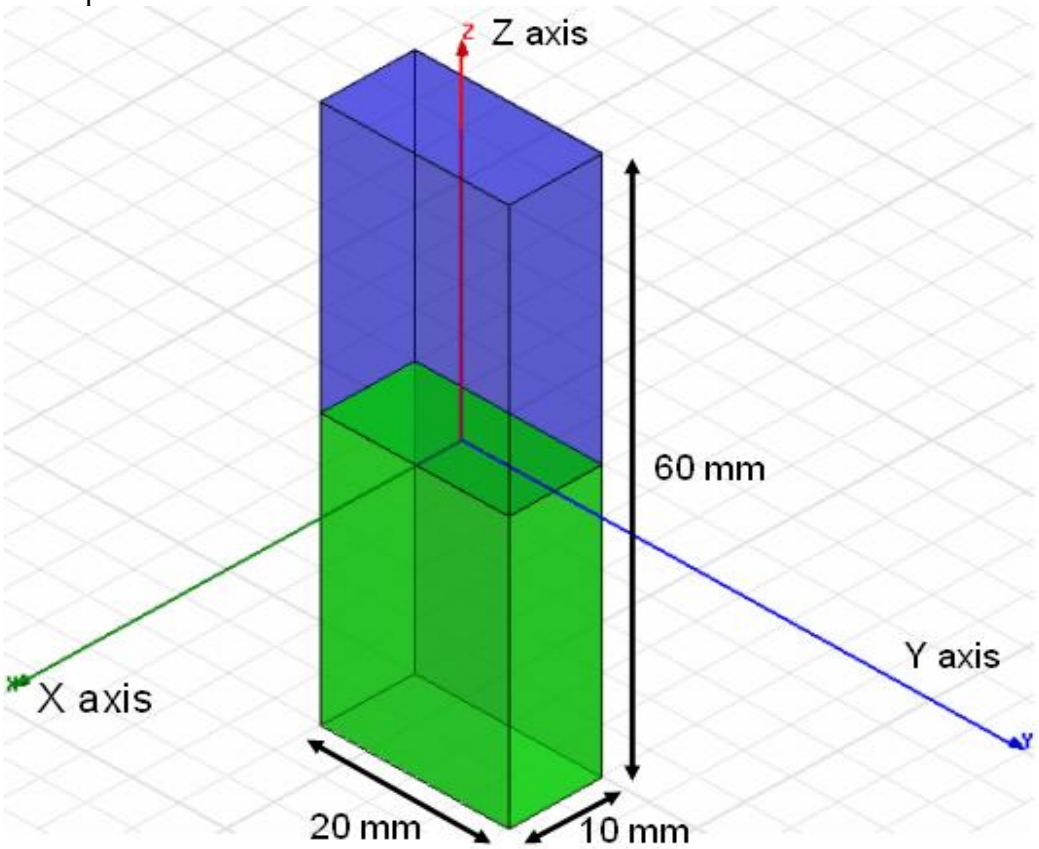

Figure 1: Waveguide filled half with vacuum and half with dielectric

In one copy of the model, all side walls were lossless metal, such that the dominant mode is the TE10 mode with propagation constant 138.75 m-1 at 10 GHz and represents the TE case in the reflection analysis. In the other copy of the model, the side walls that are parallel to the YZ plane were perfect magnetic conductors while the other walls were perfect electric conductors, such that the second mode (after a TEM mode which won't be used in this test) has propagation constant 138.75 m-1 at 10 GHz and represents the TM case in the reflection analysis.

Before simulation, the waveguides were rotated over an arbitrary angle such that no face is parallel with any coordinate plane. The waveguides were driven at 10 GHz in the proper mode.

In doing so, it is good practice to calculate all propagating modes, but the coupling between modes is expected to be negligible. Simulations were run for the cases of lossless and lossy dielectric as shown in Table 2. For the HFSS to pass the test, according to IEC 62704-1, the results need to be within 2% of the analytical values given in Table 2.

Table 2: Reflection at a dielectric interface

Re(εr)	σ (S/m)	RTE	RTE- Simulated	RTM	RTM - Simulated
4	0	0.4739	0.4739	0.1763	0.1763
4	0.2	0.4755	0.4755	0.1779	0.1779
4	1	0.5105	0.5105	0.2121	0.2121

As can be seen in table 2, HFSS produces results that are identical to the analytical results.

2.2) Canonical Benchmarks

The results for few low frequency benchmarks are summarized below. These benchmarks were used to validate the accuracy of the tool at low frequencies:

2.2.1) Dipole Antenna:

The following parameter were used in the dipole antenna to resonate at 400KHz.
Dipole length: 375 meters
Feed gap: 2.5 meters
Dipole Diameter: 5 meters

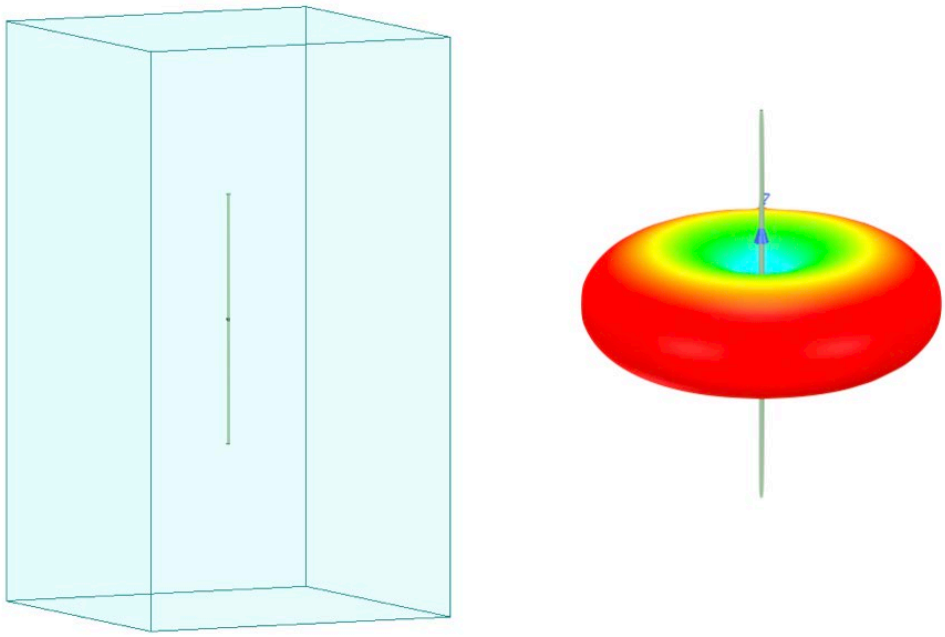

Figure 2: Dipole Antenna Model

The document IEC 62704-4 ED1 was referenced to compare the tables. Two computation methods were demonstrated as shown below to show the validity of the model.

Table 3: Simulated Dipole parameters

FEM Solver

Quantity	Simulation results	Tolerance	Satisfied?
Re(Z) at 400 KHz	**94.09**		
Im(Z) at 400 KHz	**55.62**		
Re(Z) at 320 KHz	**39.26**	$25\Omega < Re(Z) < 50\Omega$	Yes
Im(Z) at 320 KHz	**-90.52**	$-50\Omega < Im(Z) < -100\Omega$	Yes
Re(Z) at 360 KHz	**59.58**	$50\Omega < Re(Z) < 75\Omega$	Yes
Im(Z) at 360 KHz	**-18.30**	$-25\Omega < Im(Z) < 0\Omega$	Yes
Frequency for Im(Z) =0	**370**	$360MHz < f < 380MHz$	Yes
Maximum power budget error	**0.3**	$< 5\,\%$	Yes

MoM Solver

Quantity	Simulation results	Tolerance	Satisfied?
Re(Z) at 400 KHz	**98.45**		
Im(Z) at 400 KHz	**53.57**		
Re(Z) at 320 KHz	**43.31**	$25\Omega < Re(Z) < 50\Omega$	Yes
Im(Z) at 320 KHz	**-90.55**	$-50\Omega < Im(Z) < -100\Omega$	Yes
Re(Z) at 360 KHz	**65.03**	$50\Omega < Re(Z) < 75\Omega$	Yes
Im(Z) at 360 KHz	**-18.59**	$-25\Omega < Im(Z) < 0\Omega$	Yes
Frequency for Im(Z) =0	**370**	$360MHz < f < 380MHz$	Yes
Maximum power budget error	**0.02**	$< 5\,\%$	Yes

2.2.2) Toroid Inductor:

The parameters of the toroid were chosen to be
N = 20
A = 6.35e-4 m^2
R = 0.0263 m
ur = 64

The formula below gave an inductance of 139uH. The model created in HFSS gave an inductance of 139.9uH.

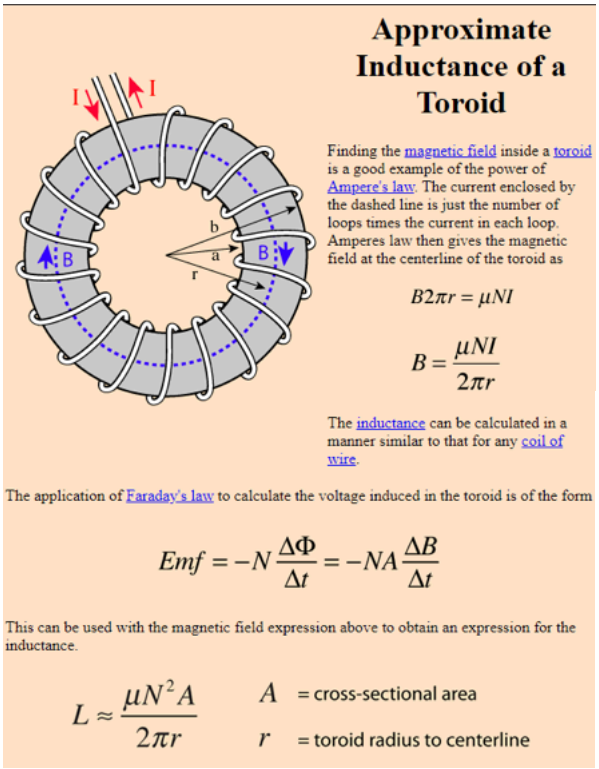

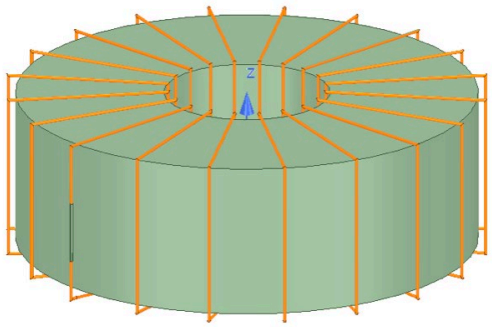

Figure 3: Toroid Model

2.2.3) Circular coil parallel to a flat, homogeneous phantom.:

The following benchmark is implemented using Equations 1-4 of the referenced Chen et al. (2014) paper and also matches Figure 6 therein scaled to 10 coil turns.

Below is the coil and phantom parameters:

Coil Diameter: 50 mm
Number of Turns: 10
RMS Current: 0.707 A (Peak current = 1 A)
Frequency: 100 kHz
Coil-to-Body Distance: 5 mm
Tissue Conductivity: 0.05 S/m
Tissue Permittivity: 1120

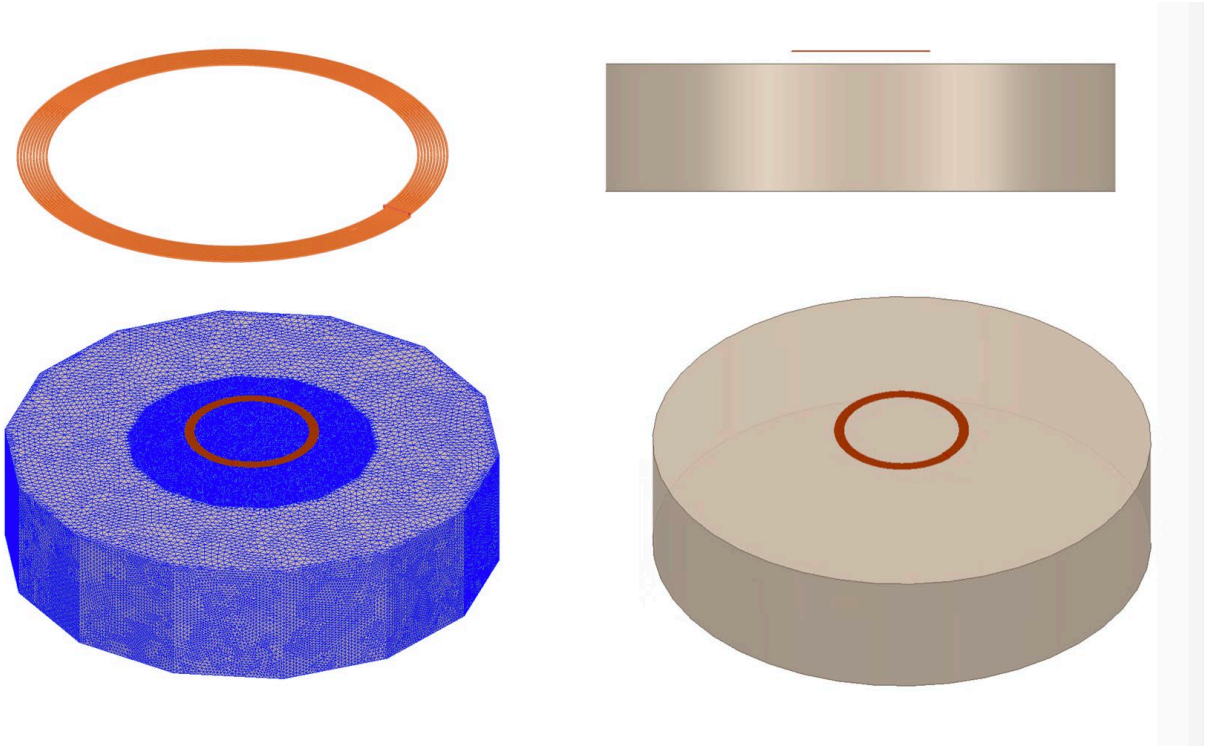

Figure 4: Current loop in front of a cuboid

The simulated spatial peak RMS electric field in tissue is 1.51 V/m compared to the analytical 1.47 V/m.

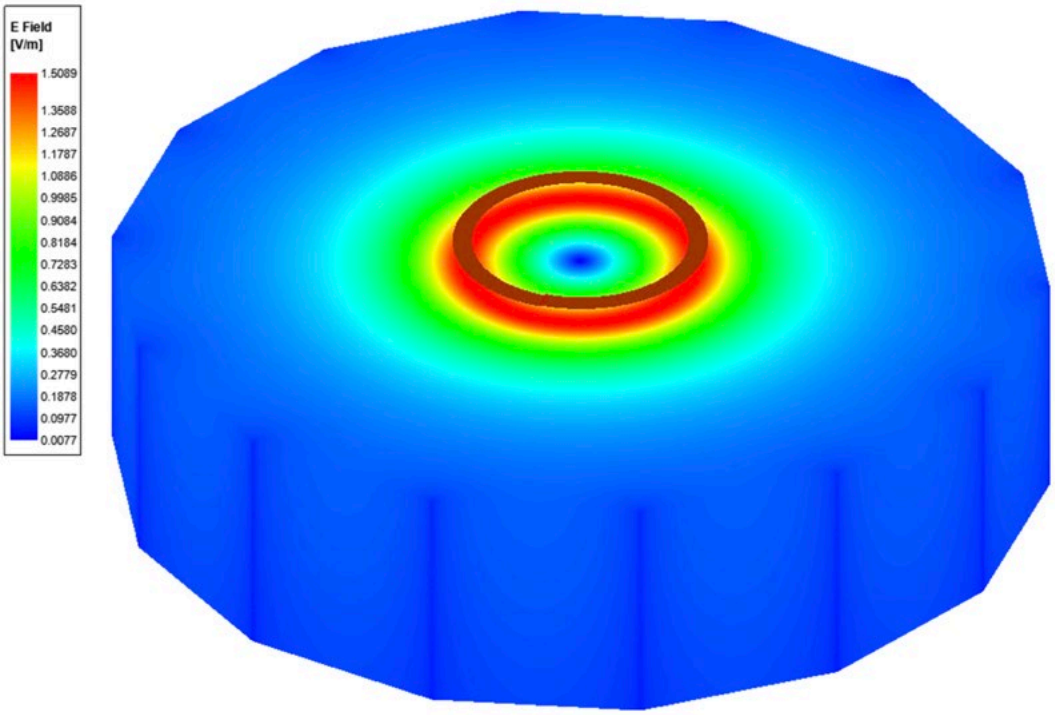

Figure 5: Current Density plot

3) Computational peak SAR from peak components & One-gram averaged SAR procedure

The calculation method for SAR follows IEEE P1528.4. Once the solver calculated the S-Parameter results, different coils can be driven and the result from the S-Parameter calculation is automatically scaled to the driving current of the coils. This result combination provides the correctly scaled power loss density in the phantom. The SAR calculation computes the local SAR first using electric field and conducting current:

$$SAR = \vec{E} \bullet \vec{J}_{conj} / (2\rho)$$

Afterwards the local SAR is averaged over a specific mass, usually 1g or 10g. As described in [IEEE P1528.4] the mass averaging is done by mapping the results to a structured hexahedral grid and afterwards the averaging scheme for FDTD per [IEEE P1528.4] is applied. The SAR calculation on the hexahedral grid is compliant with IEC 62704-1.

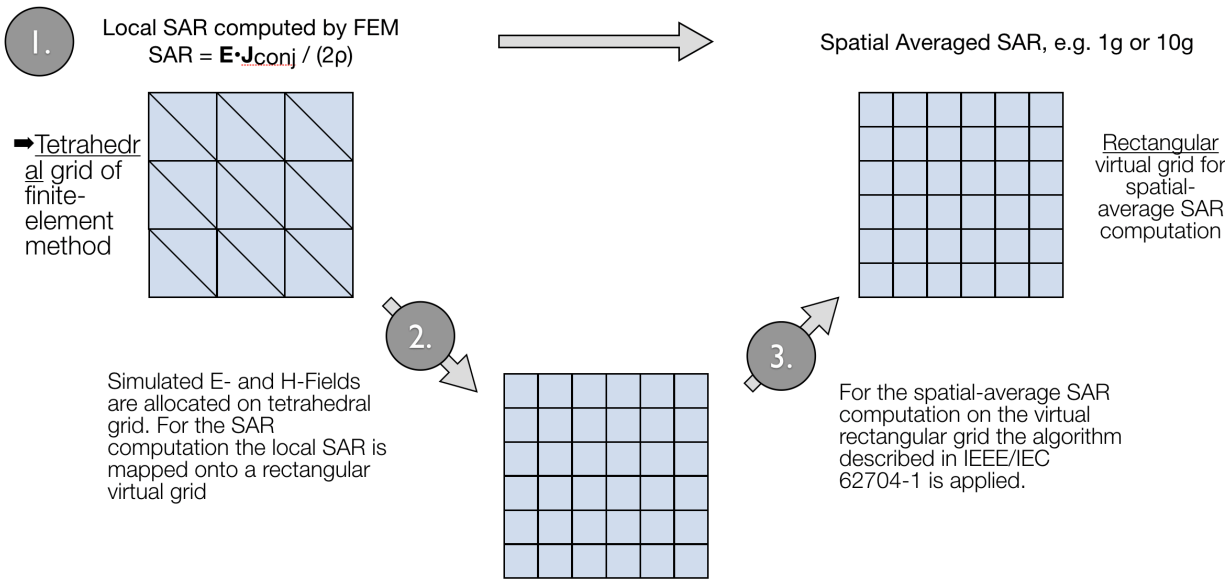

Figure 6: IEEE P1528.4 for SAR computation

4) Total Computational Uncertainty

Below is a table summarizing the budget of the uncertainty contributions of the numerical algorithm and of the rendering of the simulation setup. The table was filled using the IEC 62704-4 ED1 from 2018.
For the simulations, the extreme case where the phantom is placed directly in front of the battery is considered. Among all of the investigated conditions, the positioning generated the highest uncertainty of 8.3%. This mainly roots from the fact that based on the instruction in 7.2.2 subclause, a 0.44 mm air gap was inserted between the battery and the phantom, leading to a discontinuity. Therefore, the SAR value of the model with displaced phantom changed compared to the baseline (contact) case. Worth mentioning that since ANSYS HFSS uses a sophisticated adaptive meshing technique enhanced with an advanced initial meshing technology, the generated mesh can conform to complex geometries, well. This mitigates the artificial gap that a poor mesh could introduce between the touching objects.

Table 5. Budget of uncertainty contributions of the numerical algorithm (filled based on IEC 62704-4 ED1).

a	b	d	e	g
Uncertainty component	**Subclause**	**Probability distribution**	**Divisor f(d, h)**	**Uncertainty %**
Positioning	7.2.2	R	1,73	**8.3**
Mesh resolution	7.2.3	N	1	**0.01**
ABC	7.2.4	N	1	**0.08**
Power budget	7.2.5	N	1	**0.0**

Convergence	7.2.6	R	1,73	**0.01**
Phantom dielectrics	7.2.7	R	1,73	**0**
Combined standard uncertainty (k = 1)				**8.4**

Below is a table summarizing the budget of the uncertainty of the developed model of the EUT so far. The table was filled using the IEC 62704-4 ED1 from 2018.

Two probe separation was considered, 0mm and 30mm. The Uncertainty at 0mm is much higher because of the probe coupling to EUT.

Table 6. Measurement uncertainty table.

Probe in contact (case with highest measured H-field, Case404-Battery side):

a	**b**	**d**	**e**	**g**
Uncertainty component	**Subclause**	**Probability distribution**	**Divisor f(d, h)**	**Uncertainty %**
Uncertainty of the EUT model (based on near field distribution)	7.2.2	N	1	**46**
Uncertainty of the measurement equipment and procedure	7.2.3	N	1	**4**
Combined standard uncertainty (k = 1)				**50**

Probe 30 mm away (Case 404-Battery side):

Table 7. Measurement uncertainty when the probe is at 30 mm distance form EUT.

a	**b**	**d**	**e**	**g**
Uncertainty component	**Subclause**	**Probability distribution**	**Divisor f(d, h)**	**Uncertainty %**
Uncertainty of the EUT model (based on near field distribution)	7.2.2	N	1	**27**
Uncertainty of the measurement equipment and procedure	7.2.3	N	1	**4**

Combined standard uncertainty (k = 1)	**31**

SAR calculations are also performed using specific standard anthropomorphic model (SAM) for the use-case of the WPT device described in this report. The use-case for the WPT device is shown in below. SAM accurate model with appropriate frequency-dependent SAM tissue dielectric properties are used in the simulation [Ref. 3]. The average SAR is calculated for the worst-case scenario with peak current of 3A as the input excitation source for the coil. The average SAR value is 0.0057 W/Kg. The SAR values from anatomical model is much lower than worst case scenario used in the main section, which only impacts the uncertainty calculation in the negative direction, making the presented data in section 6 always representing worst case numbers.

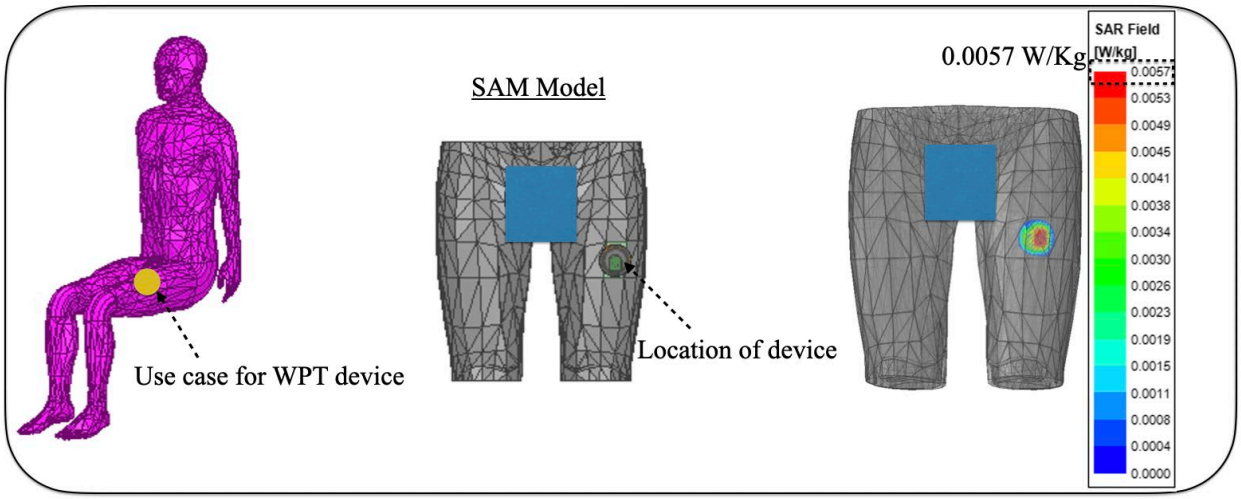

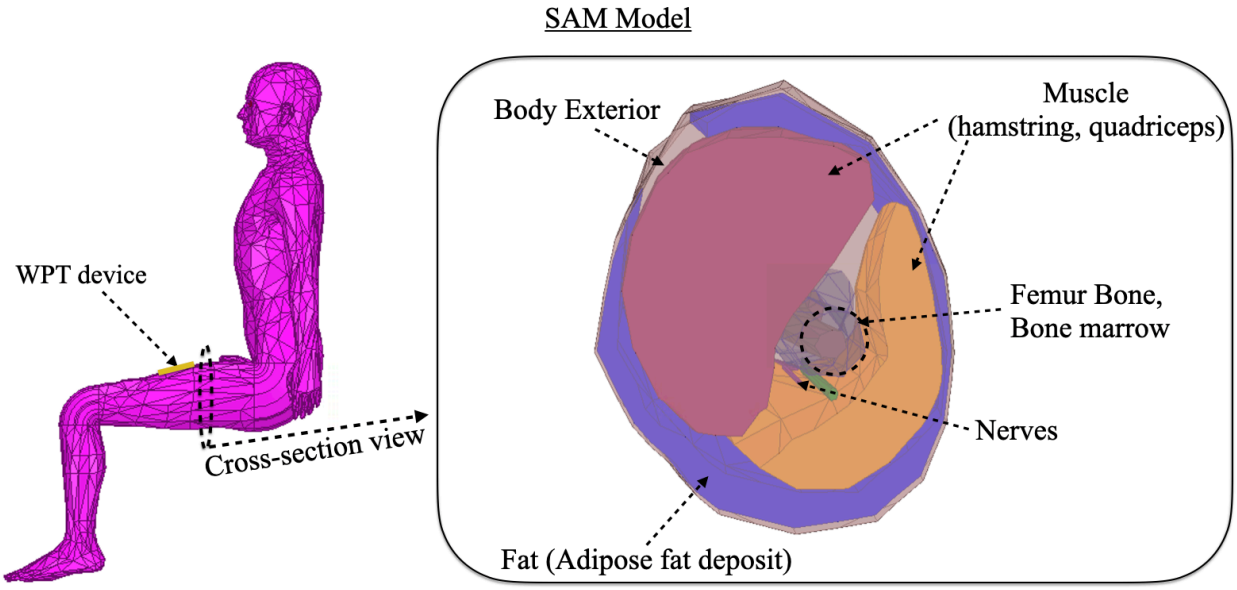

References:

1) **The electrical conductivity of human cerebrospinal fluid at body temperature, S.B. Baumann ; D.R. Wozny ; S.K. Kelly ; F.M. Meno, IEEE Transactions on Biomedical Engineering (Volume: 44 , Issue: 3 , March 1997)**
2) **C.Gabriel, S.Gabriel and E.Corthout: The dielectric properties of biological tissues: I. Literature survey, Phys. Med. Biol. 41 (1996), 2231-2249.**
3) **S.Gabriel, R.W.Lau and C.Gabriel: The dielectric properties of biological tissues: II. Measurements in the frequency range 10 Hz to 20 GHz, Phys. Med. Biol. 41 (1996), 2251-2269.**
4) **S.Gabriel, R.W.Lau and C.Gabriel: The dielectric properties of biological tissues: III. Parametric models for the dielectric spectrum of tissues, Phys. Med. Biol. 41 (1996), 2271-2293.**
5) **https://itis.swiss/virtual-population/tissue-properties/database/thermal-conductivity/**
6) **http://hyperphysics.phy-astr.gsu.edu/hbase/magnetic/toroid.html**
7) **X. L. Chen et al., "Human Exposure to Close-Range Resonant Wireless Power Transfer Systems as a Function of Design Parameters," in IEEE Transactions on Electromagnetic Compatibility, vol. 56, no. 5, pp. 1027-1034, Oct. 2014.**